Chemical Engineering Journal 351 (2018) 473–481

Contents lists available at ScienceDirect

Chemical Engineering Journal

journal homepage: www.elsevier.com/locate/cej

Thermally insulating, fire-retardant, smokeless and flexible polyvinylidene fluoride nanofibers filled with silica aerogels

Young-Gon Kim[a,1], Hyun Su Kim[b,1], Seong Mu Jo[a,*], Seong Yun Kim[c,*], B.J. Yang[b,*], Jaehyun Cho[b], Sungho Lee[a], Ji Eun Cha[b]

[a] Carbon Composite Materials Research Center, Korea Institute of Science and Technology (KIST), 92 Chudong-ro, Bongdong-eup, Wanju-gun, Jeonbuk 55324, Republic of Korea

[b] Multifunctional Structural Composite Research Center, Korea Institute of Science and Technology (KIST), 92 Chudong-ro, Bongdong-eup, Wanju-gun, Jeonbuk 55324, Republic of Korea

[c] Department of Organic Materials and Fiber Engineering, Chonbuk National University, 567 Baekje-daero, Deokjin-gu, Jeonbuk 54896, Republic of Korea

HIGHLIGHTS

- Silica aerogels filled polyvinylidene fluoride nanofibers were successfully fabricated.
- The nanofibers showed flexibility, fire-retardancy and low thermal conductivity.
- The low thermal conductivity originated from unique pore structure of the fibers.
- Precise analysis based on micro-CT was suggested for the pore structure.
- A micromechanical two-scale multiphase model was proposed for the structure.

ARTICLE INFO

Keywords:
Aerogel
Fiber
Composite
Thermal conductivity

ABSTRACT

The thermally insulating, fire-retardant, smokeless and flexible polymer nanofiber is an incredibly important material for mankind. This polymer nanofiber is expected to breed technological innovations in applications such as thermally insulated clothing and building materials. Here, we propose an electrospinning process to fabricate silica aerogel-filled polymer nanofibers by modifying the typical sol–gel chemistry process for the synthesis of silica aerogel. Silica aerogel-filled polyvinylidene fluoride (PVdF) nanofiber webs, fabricated using the proposed process, were fire-retardant, smokeless and flexible; they also exhibited a low thermal conductivity of 0.028 $W \cdot m^{-1} \cdot K^{-1}$, which was 26.3% lower than that of pure PVdF nanofiber webs. To study the unique thermal characteristics of nanofibers theoretically, a micromechanics-based, two-scale multiphase model was proposed, with consideration of fiber structure including nano and micro pores. These developments make an important contribution to bringing silica aerogel products to everyday life.

1. Introduction

First discovered by Kistler [1], an aerogel is a uniquely structured solid material that consists of a three-dimensional solid backbone with pores; aerogels have the lowest density of any known solids reported to be in the range of 0.003–0.1 $g \cdot cm^{-3}$ [2–4]. Due to their unique structure, they have also been reported to have surface areas ranging from 500–1200 $m^2 \cdot g^{-1}$, with thermal conductivities of 0.013–0.14 $W \cdot m^{-1} \cdot K^{-1}$ and dielectric constants of 1.1–2.0 [4–10]. These outstanding properties have been used extensively in aerospace applications such as thermal insulation for spacecraft [11]. However, aerogel materials have limited uses in everyday products because of their brittleness, poor mechanical properties, and challenging fabrication [12–14].

Studies on aerogels have focused mainly on improving the strength of the aerogel structure for use in insulators. Zhao et al. [14] classified three conventional methods for the efficient reinforcement of silica aerogels, namely: "(i) chemical cross-linking with reactive molecules or polymers, covalently bridging the silica nanoparticles and making the bridges of the inter-particles stronger [15,16]; (ii) incorporating individualized micro or nanoscale materials as reinforcement into the

* Corresponding authors.
E-mail addresses: smjo@kist.re.kr (S.M. Jo), sykim82@jbnu.ac.kr (S.Y. Kim), bj.yang@kist.re.kr (B.J. Yang).
[1] The authors contributed equally to this work.

https://doi.org/10.1016/j.cej.2018.06.102
Received 28 March 2018; Received in revised form 5 June 2018; Accepted 14 June 2018
Available online 15 June 2018
1385-8947/

silica matrix such as polymer nanoparticles, carbon nanotubes or fibers [17], glass fibers, ceramic fibers, or polymeric nanofibers [18]; and (iii) interpenetrating a fibrous three-dimensional scaffold within the silica matrix [19,20]." From a different perspective, some studies have discussed how to make aerogel-filled composites cheaper for applications such as insulating materials in everyday products [21,22]. Recently, Kim et al. [22] have reported that low-cost composite insulators can be developed using mass producible and inexpensive aerogel powder, which can be fabricated based on an ambient drying process without supercritical fluids. Such low-cost insulating composites were developed using different polymers, including polyimide, epoxy, and polyvinyl alcohol, but the developed materials showed a lack of flexibility, resulting in their limited use in everyday products. Ultimately, such studies can provide clues to approach thermally insulating, fire-retardant, smokeless and flexible polymer nanofibers, dream materials for mankind, which are expected to pave the way for technical innovations in such applications as insulated clothing, gloves and shoes. However, there have been very few reports on new technology or developments capable of fabricating super-insulating, fire-retardant, smokeless, flexible and aerogel-based fibers.

This study was motivated from the need to develop a technology for fabricating fire-retardant, smokeless and flexible fibers with extremely low thermal conductivity. We propose an electrospinning process to fabricate silica aerogel-filled polymer nanofibers by modifying the typical sol-gel chemistry process for the synthesis of silica aerogel. PVdF, used as the matrix, is a material that generates relatively little smoke during a fire event. We then evaluated the thermal conductivity of the fabricated nanofibers and found that the enhanced insulating properties of nanofibers stems from their unique multi-scale porous structures including micropores and nanopores. Further, in order to study the unique thermal characteristics of nanofibers theoretically, a micromechanics-based, two-scale multiphase model was proposed accounting for the multi-scale porous structures; strong agreement was observed between experimental and theoretical results within the micro and sub-micro scales.

2. Experimental

2.1. Fabrication of silica aerogel filled PVdF nanofibers

A silica aerogel-PVdF immiscible blend system was prepared in separate parts. The silica aerogel portion was synthesized from a precursor by the sol-gel method, including hydrolysis and polycondensation. Tetraethyl orthosilicate, 0.54 mol (Aldrich, St. Louis, MS, USA) was mixed with 1.08 mol of ethyl alcohol (Aldrich, St. Louis, MS, USA), 1.08 mol of distilled water, and 5 mmol of aqueous hydrochloric acid (Aldrich, St. Louis, MS, USA) under vigorous stirring. The solution showed a phase transition from opaque to transparent, and was then heated at a temperature of 95 °C in order to accelerate polycondensation. Before the polymerizing solution grew into an infinite network, N,N-dimethyl formamide (DMF, Aldrich, St. Louis, MS, USA) was added to impede further reaction and to obtain a suitable silica composition. After a brief mixing of the silica aerogel portion with PVdF (Kynar 761, Arkema, Colombes, France) and additional DMF, a transparent blend solution of silica-PVdF was produced. The silica aerogel-PVdF solution was charged by high direct current voltage and released through a metallic capillary tube as shown in Fig. 1. The ejected solution underwent elongation, evaporation, and solidification; it eventually formed a fiber. The fibers were collected on a grounded layer, which enabled the sheet-like formation of a fibrous mat. By feeding the solution very quickly, and/or maintaining a short tip-to-collector distance, the mat was formed with solvent inside because the solvent did not have sufficient time to evaporate during the electrospinning process. The as-prepared mat was instantly treated with supercritical fluid before undergoing aging. The silica-PVdF sheet was placed in a high-pressure resistant vessel that was filled with carbon dioxide gas at a gauged pressure of up to 2000 psi; this was followed by heating at 45 °C for 5 h. For comparison, a separately aged sample was dried under ambient conditions for 3 days. The processing conditions are summarized in Table 1.

2.2. Characterization of silica aerogel-filled PVdF nanofibers

The content of the silica aerogel in the fabricated nanofibers was analyzed by performing thermogravimetric analysis (TGA, Q50, TA Instrument, New Castle, DE, USA) in open air at temperatures ranging from room temperature to 800 °C with a heating rate of 10 °C·min^{-1}. Fourier transform infrared spectroscopy (FT-IR, Nicolet 6700, Thermo Scientific, MA, USA) and X-ray photoelectron spectroscopy (XPS, K-Alpha, Thermo Scientific, Massachusetts, USA) were used to analyze the chemical composition of the fabricated silica aerogel-PVdF nanofibers. FT-IR spectra were measured in the range of 500–4000 cm^{-1} at a resolution of 16 cm^{-1}. XPS spectra were obtained with an Al X-ray source under a pressure of 1×10^{-8} Pa. The morphologies of the fabricated nanofibers were observed with a transmission electron microscope (TEM, Tecnai F20, FEI Corp., OR, USA) and a field emission scanning electron microscope (FE-SEM, Nova NanoSEM 450, FEI Corp., OR, USA and Veirous 460L, FEI Corp., OR, USA). TEM observations were carried out at 120 kV. The nanofibers were coated with platinum under vacuum for 200 s using a sputter coating machine (Ion Sputter E-1030, Hitachi High Technologies, Tokyo, Japan); the FE-SEM observations were subsequently performed. Energy dispersive spectroscopy (EDS) analysis was additionally conducted with a resolution of 127 eV. The thermal conductivity of the electro-spun nanofiber web was measured based on ISO standard 22007-2 using a thermal conductivity instrument (TPS 2500S, Hot Disk ab, Gothenburg, Sweden). A nickel double coil comprising a plane sensor was sandwiched between two nanofiber sheets. The resistance or the temperature rise of the nickel double coil was recorded during electrical heating. The analyzer yields information about the thermal diffusivity, thermal conductivity, and specific heat per certain volume of the sample sheet.

2.3. Porosity characterization of silica aerogel filled PVdF nanofibers

The fabricated nanofiber web consists of micropores between fibers and nanopores inside the fibers. Unfortunately, the analysis to directly measure the nanopores of the fabricated nanofiber web is very difficult due to technical limitations. In this study, to overcome this difficulty, the entire pore structure was determined by measuring apparent porosity and the micro pores. The apparent porosity of the electro-spun nanofiber web was calculated using the following equation:

$$P(\%) = (1-P_M)/P_P \times 100 \quad (1)$$

in which P is the apparent porosity, P_M is the density of the pristine PVdF nanofiber web, and P_P is the density of the silica aerogel-filled nanofiber web. X-ray micro-computed tomography (micro-CT, Skyscan 1172, Bruker Co, Billerica, MD, USA) was used to measure and identify the micropores between the fabricated nanofibers. Measurements were carried out at a size of 4000 × 2664 pixels, and the X-ray source was operated at 36 kV and 222 mA under normal pressure.

3. Theoretical approach

The homogenized thermal characteristics of the PVdF nanofiber

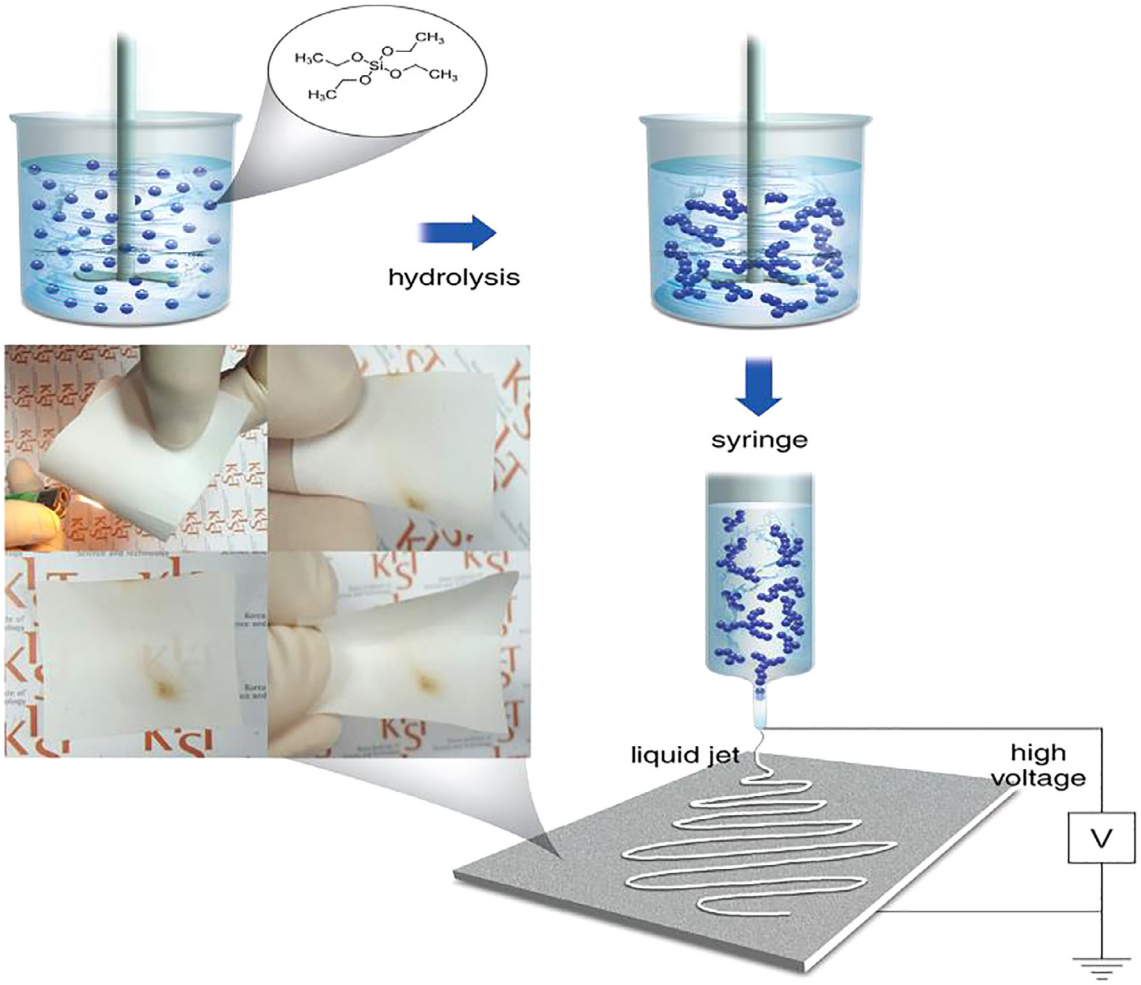

Fig. 1. Schematic for the proposed electrospinning of the silica aerogel-filled nanofibers.

Table 1
Conditions and properties of the electro-spun PVdF nanofibers.

No	Aerogel content (wt%)	TCD[a)] (cm)	FRS[b)] (μL/min)	Drying method	Porosity (%)	Micro Porosity (%)	Nano Porosity (%)	Thermal conductivity (W/m·K)
1	37	5	60	CO_2	72.6	40.5	32.1	0.051
2	37	10	60	CO_2	74.7	45.2	29.5	0.052
3	37	15	60	CO_2	90.7	63.7	27.0	0.034
4	64	5	60	CO_2	76.2	44.3	31.9	0.059
5	64	7	60	CO_2	79.9	45.2	34.7	0.050
6	64	15	60	CO_2	84.9	52.1	32.8	0.042
7	37	15	10	CO_2	91.8	69.3	22.5	0.028
8	64	15	10	CO_2	90.9	66.8	24.1	0.032
9	52	15	60	Air	86.8	53.3	33.5	0.032
10	64	15	60	Air	90.9	65.3	25.6	0.032
11	0	15	10	Air	83.3	75.6	7.7	0.038
12	52	15	60	CO_2	88.5	56.1	32.4	0.036
13	52	15	60	Air	88.5	55.0	33.5	0.037

[a)] Tip-to-collector distance.
[b)] Feed rate of solution.

web with silica aerogel are formulated based on the ensemble-volume-averaged method [23]. Herein, a two scale composite consisting of the microscopic domain (Ω_1) and the nanoscopic domain (Ω_2) is considered in order to adequately model the unique characteristics of the present composite material. The purpose of dividing the domain is to more effectively describe the properties of nanoscale voids. On the macro perspective, the pores inside the composites mainly exist in microscale; however, nanoscale pores are also present at sizes very close to the single PVdF fibers with aerogel. According to the literature [24,25], nanoscale pores are formed from gases with unique thermal properties that differ from air. The combination of micro- and nano-gaseous characteristics affects the overall thermal properties of the composite.

For the theoretical analysis of the complex system, the present composite is assumed to be divided into five phases of two domains as follows: Ω_1 is composed of a PVdF matrix (phase 0) and micro porosity (phase 1), and Ω_2 is composed of single PVdF fiber (phase 2), silica aerogel (phase 3), and nano porosity (phase 4). The illustration of the abovementioned theoretical schematic is represented in Fig. 2.

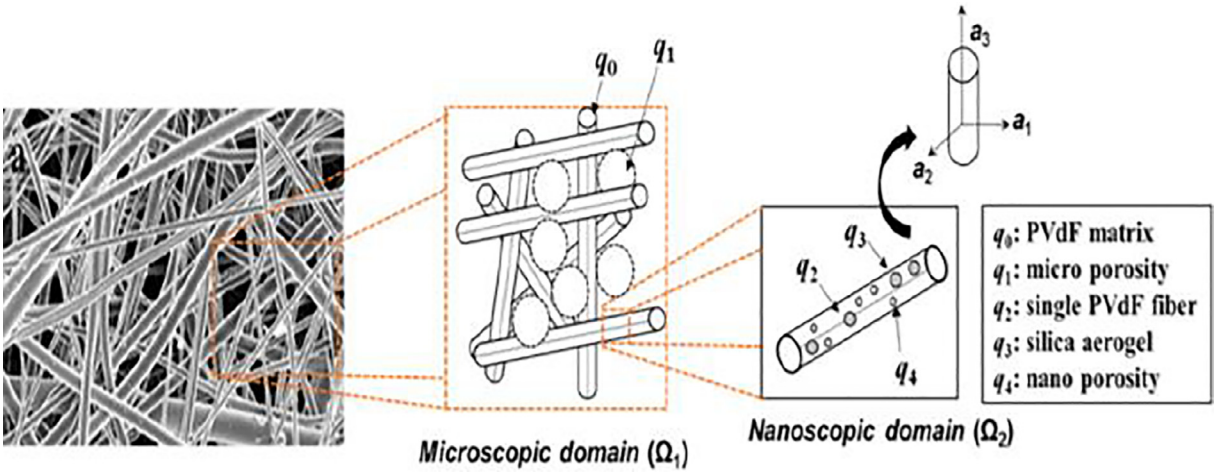

Fig. 2. Schematic illustration representing multi-phase micro and nanostructures of PVdF nanofiber web containing silica aerogel.

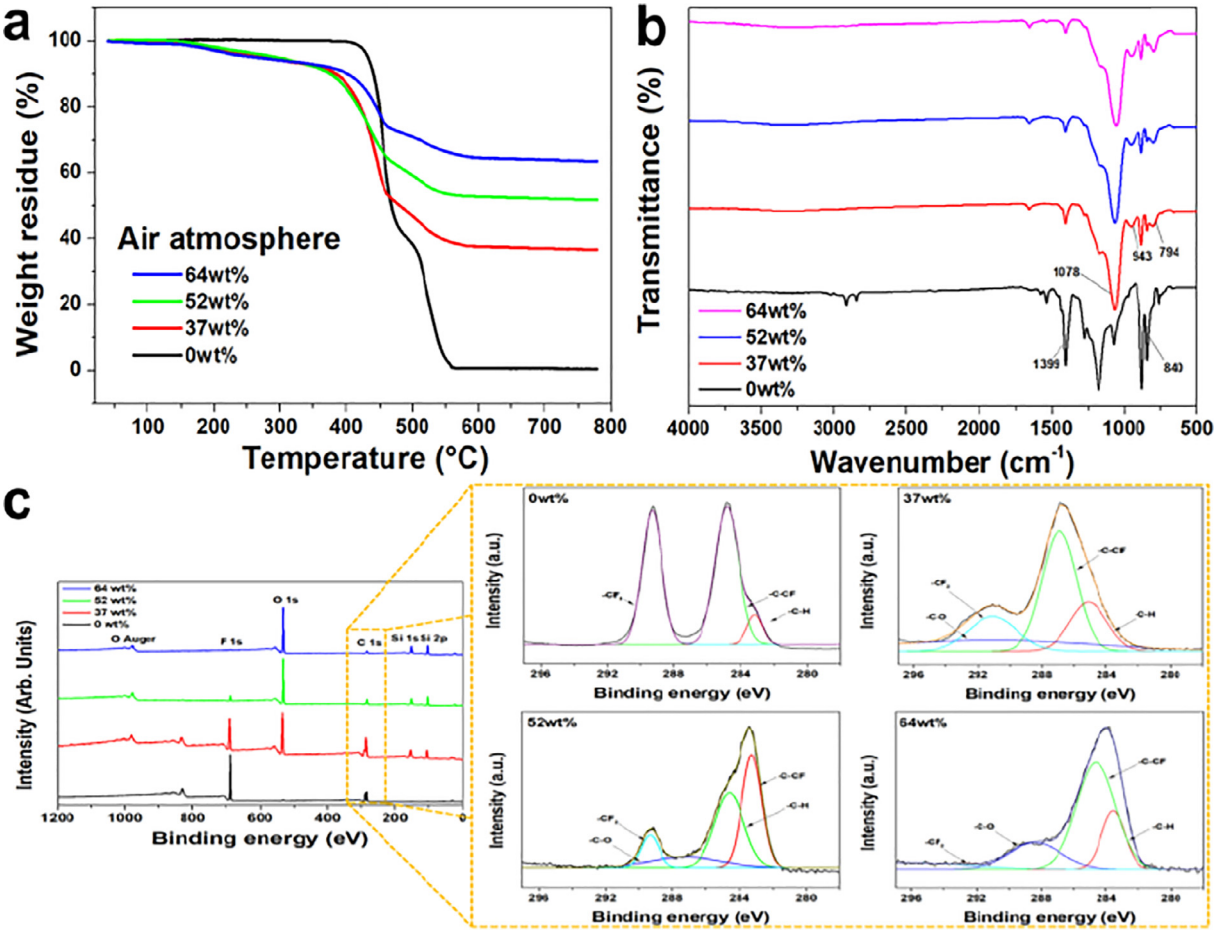

Fig. 3. Chemical composition of the fabricated PVdF and silica aerogel-filled PVdF nanofibers. (a) TGA thermogram for measuring filler contents, (b) FT-IR and (c) XPS spectra for analyzing synthesis of silica portion.

Following Hatta and Taya [26,27] and Ju and Chen [23], the elastic and thermal relationships are mutually compatible and interchangeable (e.g., stiffness to thermal conductivity, stress to heat flux, strain to thermal gradient), and thus, the following micromechanics-based framework can be constructed for the composites as [28]

$$\mathbf{K}^* = \mathbf{K}_0\cdot[\mathbf{I} + \{\langle\boldsymbol{\phi}_1(\mathbf{S}_1 + \mathbf{A}_1)^{-1}\rangle\cdot[\mathbf{I}-\langle\boldsymbol{\phi}_1\mathbf{S}_1\cdot(\mathbf{S}_1 + \mathbf{A}_1)^{-1}\rangle]^{-1}\}] \text{ at } \boldsymbol{\Omega}_1 \quad (2)$$

with

$$\mathbf{K}_0 = \mathbf{K}_2\cdot\left[\mathbf{I} + \sum_{r=3}^{4}\{\boldsymbol{\phi}_r(\mathbf{S}_r + \mathbf{A}_r)^{-1}\cdot[\mathbf{I}-\boldsymbol{\phi}_r\mathbf{S}_r\cdot(\mathbf{S}_r + \mathbf{A}_r)^{-1}]^{-1}\}\right] \text{ at } \boldsymbol{\Omega}_2 \quad (3)$$

where $\mathbf{K}^*$ denotes the effective thermal conductivity of the PVdF nanofiber web containing silica aerogel and $\mathbf{K}_r$ ($r = 0,\ldots, 4$) is the thermal

conductivity of the *r*-phase. $< \cdot >$ denotes the randomly oriented fiber, **I** represents the identity tensor, and the concentration tensor $\mathbf{A}_r$ is defined as

$$\mathbf{A}_1 = (\mathbf{K}_1 - \mathbf{K}_0)^{-1} \cdot \mathbf{K}_0, \ \mathbf{A}_r = (\mathbf{K}_r - \mathbf{K}_2)^{-1} \cdot \mathbf{K}_2 \quad (r = 3 \text{ and } 4) \tag{4}$$

$\mathbf{S}_r$ (r = 3, 4) is the second rank tensor $\boldsymbol{S}_{ij}$, which can be defined as [27]

$$\mathbf{S}_r = \int \mathrm{G}(x - x')dx \tag{5}$$

where G(X) is Green's function in a homogeneous matrix, and can be expressed as

$$S_{ij} = \frac{a_1 a_2 a_3}{4} \frac{\partial^2}{\partial x_i x_j} \int_0^\infty \left[\left(\frac{x_1^2}{a_1^2 + s} + \frac{x_2^2}{a_2^2 + s} + \frac{x_2^2}{a_2^2 + s} \right) \frac{1}{(\Delta s)} \right] ds \tag{6}$$

After length but straightforward algebra, the spherical voids of *r*-phase can be derived as follows

$$\mathbf{S}_3 = \mathbf{S}_4, \ (S_{11})_{3,4} = (S_{22})_{3,4} = (S_{33})_{3,4} = \frac{1}{3} \tag{7}$$

where a_x (x = 1, 2, 3) signify the length of inclusions along the *x*-axis (Fig. 2). In the present study, the shape of voids is assumed to be a perfect sphere, and the components of $\mathbf{S}_{3,4}$ can be simply defined as 1/3.

4. Results and discussion

4.1. Structure of silica aerogel filled PVdF nanofibers

As shown in Fig. 1, the tetraethyl orthosilicate ($Si(OR)_4$, where $R = C_2H_5$) as a precursor for the sol-gel process was readily hydrolyzed by water and the speed of the hydrolysis was controlled by the concentration of water in ethanol and catalyst, hydrochloric acid, and the stirring conditions. When the colloidal solution was formed (sol), which could further form an integrated network (gel), these were mixed with a PVdF solution to be electro-spun. During the sol formation step, the alkoxide groups (OR) from the $Si(OR)_4$ are replaced with hydroxyl groups (OH). Subsequently, a polycondensation reaction causes the intermediate silanol species to form a network via siloxane bonds (Si—O—Si) with water and alcohol as byproducts during the electrospinning.

To analyze the chemical composition of the fabricated PVdF and silica aerogel filled PVdF nanofibers, TGA, FT-IR and XPS analyses were performed. It was confirmed from the TGA results in Fig. 3a that the target content of the filler summarized in Table 1, was accurately obtained in the fabricated silica aerogel filled nanofibers. As seen in Fig. 3b, the characteristic peaks of α-crystal at 766 and 855 cm^{-1}, β-crystal at 840 cm^{-1}, C-F stretching at 1155 and 1230 cm^{-1}, and C—H deformation at 1378 cm^{-1} appeared in the FT-IR spectrum of the PVdF nanofiber. Three new characteristic peaks of symmetric Si—O—Si stretching at 794 cm^{-1}, asymmetric Si—O—Si stretching at 1078 cm^{-1}, and Si—OH stretching at 943 cm^{-1} were observed in the FT-IR spectra of silica aerogel-filled PVdF nanofibers [29]. It can be clearly observed in Fig. 3c that the XPS spectrum of the PVdF nanofiber contains only C1s and F1s peaks. New O1s, Si1p, and Si2p peaks were observed in the spectrum of the silica aerogel filled PVdF nanofibers, indicating the successful synthesis and incorporation of silica in the silica aerogel-filled PVdF nanofibers [30].

Uniquely structured nanofibers containing silica aerogel were fabricated, as shown in FE-SEM and TEM images in Fig. 4. As shown in Fig. 4a and b, statistical analysis revealed that the nanofibers were 200–900 nm in diameter. On the surface of the nanofibers, the pore structure of the silica aerogel was clearly observed (Fig. 4c) and the chemical composition was reaffirmed by the EDS elemental maps of F and Si distributions (Fig. 4d and e), indicating that three-dimensional silica aerogel structures of several tens-of-nano- to nano-sized existed in a well-dispersed form. As shown in TEM results in Fig. 4f, the inner layers of the nanofibers were composed of polymer domains as the sea component and many silica aerogels as the island components. Therefore, it was observed that the silica component introduced into the fiber was a well-dispersed aerogel structure, and it was confirmed that the nanofiber with uniformly dispersed silica aerogel was successfully fabricated.

The thermal conductivity of polymer fibers containing inorganic matter depends on phonon transport; the phonon transport in nanomaterials is known to be determined by the interfacial thermal resistance [31–33]. Aerogel-containing nanofibers are thought to have outstanding insulating performance (a low thermal conductivity) by virtue of their multi-scale porous structures, which include micropores and nanopores. As shown in Fig. 5 and video S1, the pore structure of the nanofiber can be divided into the micropore between the nanofibers and the nanopore inside the fiber. Unfortunately, the analysis to directly measure the nanopore of the fabricated nanofibers is very difficult due to technical limitations, but it is possible to determine apparent porosity based on calculations using density, and micro porosity using X-ray micro-computed tomography (micro-CT). Additionally, nano porosity can be regarded as the result of subtracting the micro porosity from the apparent porosity as summarized in Table 1. Therefore, the thermal conductivity of the nanofiber filled with silica aerogel should be understood as based on precise measurements and theoretical calculations for the multi-scale porous structures.

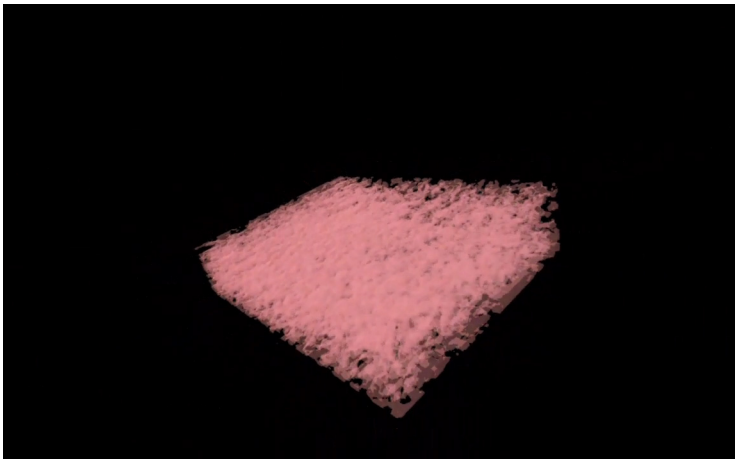

video S1.

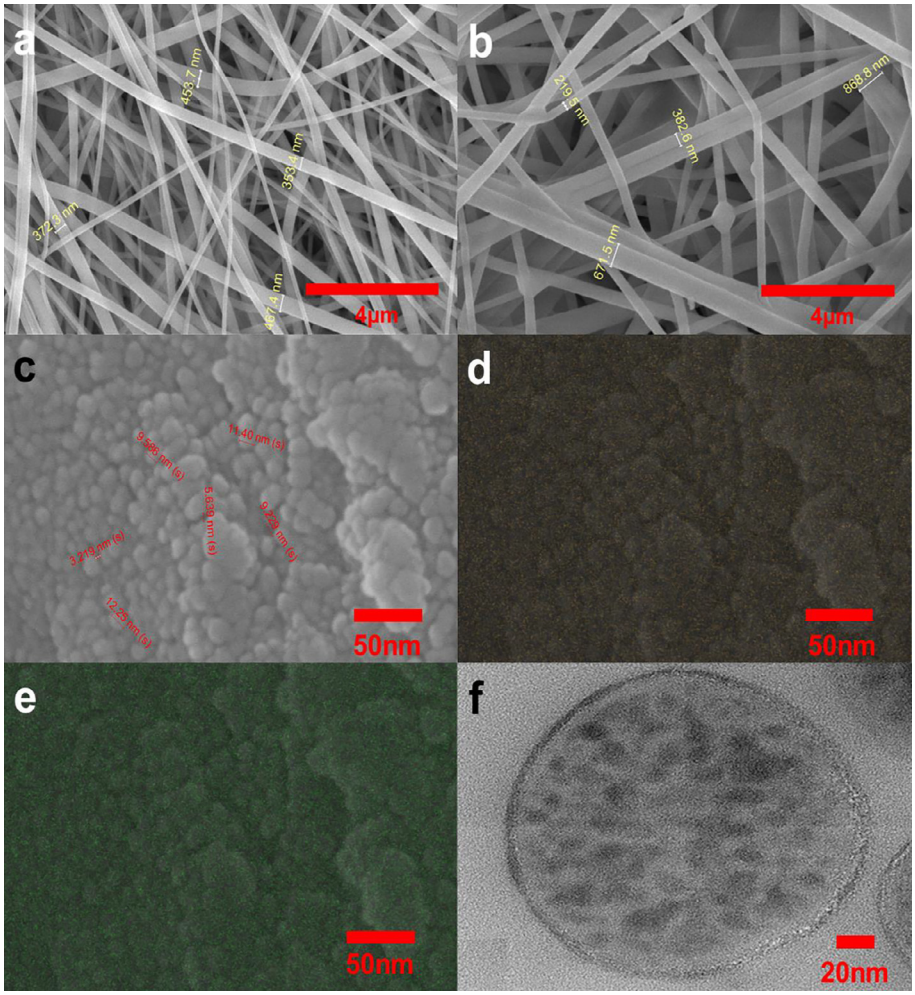

Fig. 4. Morphological structure of the fabricated PVdF and silica aerogel-filled PVdF nanofibers. FE-SEM images of the nanofibers filled (a) without aerogels, (b) with aerogels of 37 wt%, (c) with aerogels of 37 wt% for surface morphology, (d) EDS F map, (e) EDS Si map and (f) TEM image of cross section of the nanofibers filled with aerogels of 37 wt%.

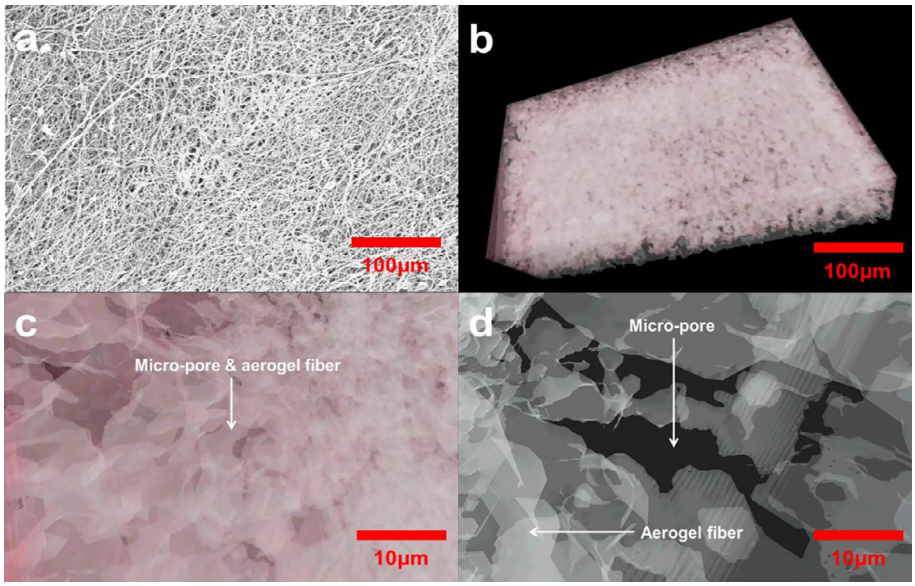

Fig. 5. Multi-scale porous structures of the fabricated silica aerogel-filled PVdF nanofibers. (a) Nano-web FE-SEM image, (b) micro-CT images, and (c, d) fiber portion (white) and micro-pore (red and black) of the nanofibers filled with aerogels of 37 wt%.

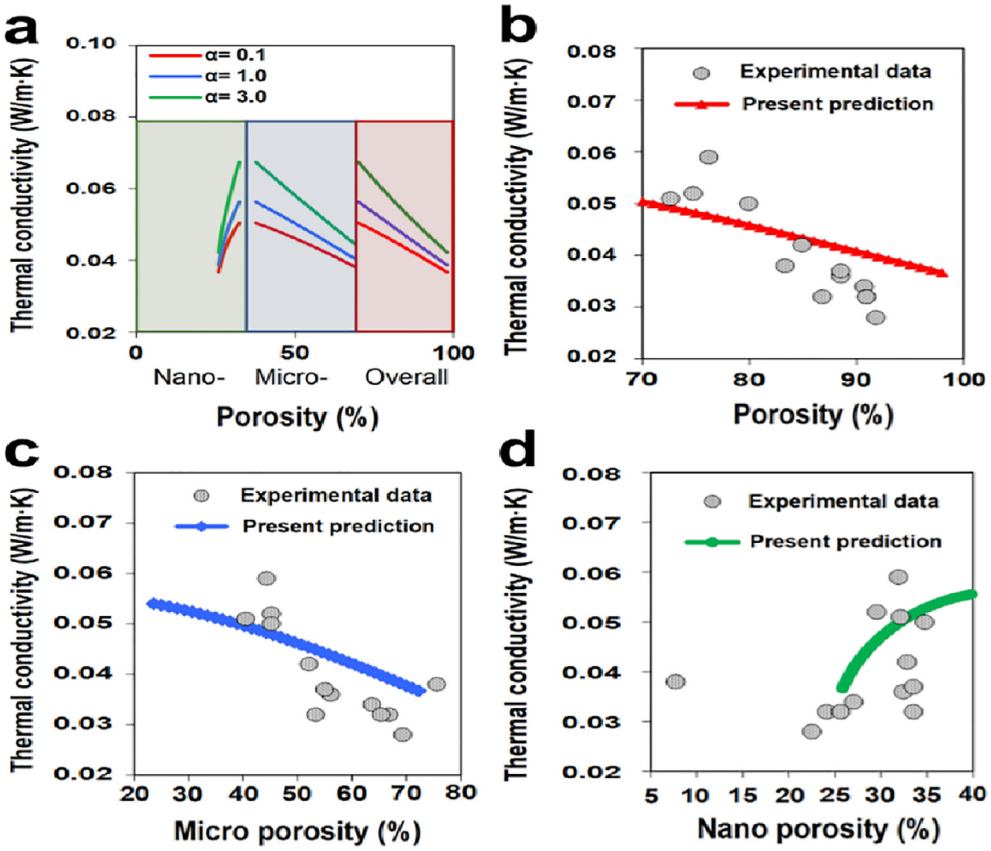

Fig. 6. Thermal conductivity of the fabricated PVdF and silica aerogel-filled PVdF nanofibers: (a) The simulated results of parametric study and (b, c, d) experimental comparisons with respect to the porosity properties.

To investigate the effectiveness of the proposed analytical model, the predictions of thermal conductivities of PVdF nanofiber webs with different constituents are compared with experimental data. The calculation of Ω_2, which accounts for the influence of nanoscale substances, is carried out initially, and the adopted materials constants for the simulation are: $K_2 = 0.12\,W{\cdot}m^{-1}{\cdot}K^{-1}$ and $K_3 = 0.02\,W{\cdot}m^{-1}{\cdot}K^{-1}$ [7,34],. The thermal conductivity of nano porosity (K_4) can vary with respect to the composition of composites, and no literature related to the present material system could be found. However, the value will have a certain relationship with the thermal conductivity of general air, and we assume that K_4 is defined as $K_4 = \alpha{\cdot}K_1$. The diameter of PVdF nanofiber is obtained by applying the average value, 550 nm.

The effective thermal conductivity at Ω_1 can be calculated by substituting the value of K_0 into the effective framework equation given in the Methods and Materials section. We adopt the following thermal conductivity micro porosity (K_1) for the simulation: $K_1 = 0.024\,W{\cdot}m^{-1}{\cdot}K^{-1}$. In addition, the total volume fraction ($\phi_{total} = 1.0$) of composite can be expressed as

$$\phi_{total} = \phi_{porosity} + \phi_{silica\ aerogel} + \phi_{PVdF} \tag{8}$$

and the volume fraction of $\phi_{porosity}$ is composed of

$$\phi_{porosity} = \phi_{micro\ porosity} + \phi_{nano\ porosity} = \phi_1 + \phi_4 \tag{9}$$

where ϕ_1 and ϕ_4 are found to have the following relation through experimental measurement results:

$$\begin{aligned} \phi_1 &= -0.004(\phi_{porosity})^2 + 2(\phi_{porosity}) - 78.5 \\ \phi_4 &= 0.004(\phi_{porosity})^2 + (\phi_{porosity}) + 78.5 \end{aligned} \tag{10}$$

In addition, $\phi_{silica\ aerogel}$ can be calculated by converting the weight fraction of silica aerogel listed in Table 1. The volume fraction ϕ_{PVdF} is regarded as the remaining value obtained by subtracting $\phi_{porosity}$ and $\phi_{silica\ aerogel}$ from ϕ_{total}.

Prior to experimental comparisons, a simple numerical analysis is performed on α, which is the only model constant in the present model. Fig. 6a shows the effect of nano porosity on the thermal conductivity of the composite for three different scales of pores. Considering the larger value of α means higher thermal conductivity of nano porosity, the increase in thermal conductivity of nano porosity leads to an increase in the overall thermal conductivity at all scales. Interestingly, porosity at the nanoscale serves to improve the thermal conductivity; however, the opposite result is predicted for the other two scales (micro and total). From the overall viewpoint, the increase in pore size leads to a decrease in effective thermal conductivity of composite, which is thought to be due to the effect of pore size on the microscale being greater than that on the nanoscale.

A comparative study is then carried out between the theoretical results and the experimental data, as shown in Fig. 6. To simulate the experimental results according to the pore scale, predictions with respect to overall porosity, micro porosity, and nano porosity are illustrated in Fig. 6b-d, respectively. It should be noted that the same model constant α = 0.1 was applied in all cases of the comparisons. Although there is some divergence, it is in good agreement with all cases and supports the validity of the proposed method.

In the electrospinning process, the tip-to-collector distance (TCD) and the feed rate of solution (FRS) are typical process conditions that allow the porosity of the resulting nanofibers to be adjusted. Figs. S1 and S2 show how the thermal conductivity of the nanofibers varies with the TCD and FRS factors in the electrospinning process. The water content of the fabricated nanofibers is generally known to decrease with increasing TCD [35]; the dryness of the silica aerogel-containing PVdF nanofibers is considered to be a significant factor in the thermal conductivity. As the TCD increased, the porosity of the nanofibers increased and their thermal conductivity decreased. When the FRS was

reduced from 60 to 10 μm·min^{-1}, the thermal conductivity of the nanofibers decreased by approximately 20%, and under the same conditions, the insulating performance showed an improvement of 20–30% compared with the thermal conductivity (0.038 W·m^{-1}·K^{-1}) of the PVdF nanofibers prepared without silica aerogel inside. Therefore, the TCD and FRS are thought to have acted as important process factors that influenced the dryness of the aerogel-containing nanofibers, and determined the porosity and thermal conductivity of the fabricated nanofibers.

4.2. Fire-retardant, smokeless and flexible properties of silica aerogel filled PVdF nanofibers

Fig. S3 and video S2 illustrate the excellent fire-retardant properties and flexibility of the fabricated nanofibers. Our tests found that when the nanofiber sheet came into contact with flames, the PVdF nanofiber web without silica aerogel generated no smoke but contracted immediately and lost its fire-retardant properties, whereas nanofibers with silica aerogel inside exhibited excellent fire-retardant. Thanks to the properties of the PVdF matrix, it was possible to make smokeless nanofibers; the incorporated silica aerogel imparted fire-retardant properties to the nanofibers. In the end, we were able to fabricate fire-retardant, smokeless and flexible nanofibers with a low thermal conductivity of 0.028 W·m^{-1}·K^{-1}.

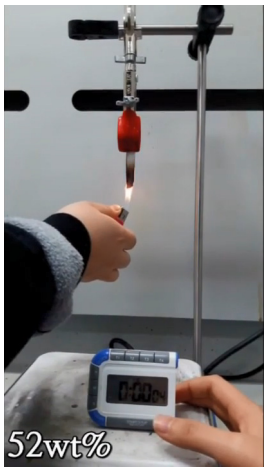

video S2.

5. Conclusions

The present work proposed a modified sol-gel chemistry process for fabricating uniquely structured super-insulating, fire-retardant, smokeless and flexible polymer nanofibers filled with silica aerogel. Three-dimensional silica structures were formed inside the nanofibers; these existed in a well-dispersed form, and silica aerogel pores were clearly observed. From the study findings, it was concluded that the porosity of the nanofibers is the most important physical factor determining the thermal conductivity. The aerogel-containing nanofibers fabricated in this study exhibited outstanding insulating performance (a low thermal conductivity) by virtue of their multi-scale porous structures, including micropores and nanopores. Considering the nanofiber structure with nano- and micropores, a two-scale multi-phase model was proposed and the improved thermal characteristics were theoretically analyzed. The response of the proposed material was moderately well predicted by the micromechanical model. The TCD and FRS were found to act as key processing factors that allowed the control of the porosity and thermal conductivity of the nanofibers. The characteristics of the PVdF matrix made it possible to fabricate smokeless nanofibers; the incorporated silica aerogel imparted fire-retardant properties to the nanofibers. Consequently, we succeeded in fabricating thermally insulating, fire-retardant, smokeless and flexible PVdF nanofibers.

Acknowledgements

This research was supported by Korea Institute of Science and Technology (KIST) Institutional Program, Basic Science Research Program (2017R1C1B5077037) through the National Research Foundation of Korea (NRF) funded by the Ministry of Education and the Industrial Technology Innovation Program (10082586) Funded by the Ministry of Trade, Industry & Energy of Korea.

Appendix A. Supplementary data

Supplementary data associated with this article can be found, in the online version, at https://doi.org/10.1016/j.cej.2018.06.102.

References

[1] S.S. Kistler, Coherent expanded aerogels and jellies, Nature 127 (1931) 741.
[2] S.S. Prakash, C.J. Brinker, A.J. Hurd, S.M. Rao, Silica aerogel films prepared at ambient pressure by using surface derivatization to induce reversible drying shrinkage, Nature 374 (1995) 439–443.
[3] A.C. Pierre, G.M. Pajonk, Chemistry of aerogels and their applications, Chem. Rev. 102 (2002) 4243–4265.
[4] H. Maleki, Recent advances in aerogels for environmental remediation applications: a review, Chem. Eng. J. 300 (2016) 98–118.
[5] X. Lu, M.C. Arduini-Schuster, J. Kuhn, O. Nilsson, J. Fricke, R.W. Pekala, Thermal conductivity of monolithic organic aerogels, Science 255 (1992) 971–972.
[6] N. Hüsing, U. Schubert, Aerogels-airy materials: chemistry, structure, and properties, Angew. Chem. Int. Ed. 37 (1998) 22–45.
[7] A.S. Dorcheh, M.H. Abbasi, Silica aerogel; Synthesis, properties and characterization, J. Mater. Process. Technol. 199 (2008) 10–26.
[8] R. Baetens, B.P. Jelle, A. Gustavsen, Aerogel insulation for building applications: a state-of-the-art review, Energy Build. 43 (2011) 761–769.
[9] H. Sai, J. Xiang, L. Cui, J. Jiao, C. Zhao, Z. Li, F. Li, Flexible aerogels based on an interpenetrating network of bacterial cellulose and silica by a non-supercritical drying process, J. Mater. Chem. A 1 (2013) 7963–7970.
[10] J. Wang, Y. Zhang, X. Zhang, Reversible superhydrophobic coatings on lifeless and biotic surfaces via dry-painting of aerogel microparticles, J. Mater. Chem. A 4 (2016) 11408–11415.
[11] J.P. Randall, M.A.B. Meador, S.C. Jana, Tailoring mechanical properties of aerogels for aerospace applications, ACS Appl. Mater. Interfaces 3 (2011) 613–626.
[12] S. Yun, H. Luo, Y. Gao, Ambient-pressure drying synthesis of large resorcinol–formaldehyde-reinforced silica aerogels with enhanced mechanical strength and superhydrophobicity, J. Mater. Chem. A 2 (2014) 14542–14549.
[13] H. Maleki, L. Durães, A. Portugal, Synthesis of mechanically reinforced silica aerogels via surface-initiated reversible addition-fragmentation chain transfer (RAFT) polymerization, J. Mater. Chem. A 3 (2015) 1594–1600.
[14] S. Zhao, Z. Zhang, G. Sèbe, R. Wu, R.V.R. Virtudazo, P. Tingaut, M.M. Koebel, Multiscale assembly of superinsulating silica aerogels within silylated nanocellulosic scaffolds: Improved mechanical properties promoted by nanoscale chemical compatibilization, Adv. Funct. Mater. 25 (2015) 2326–2334.
[15] M.A.B. Meador, E.F. Fabrizio, F. Ilhan, A. Dass, G. Zhang, P. Vassilaras, J.C. Johnston, N. Leventis, Cross-linking amine-modified silica aerogels with epoxies: mechanically strong lightweight porous materials, Chem. Mater. 17 (2005) 1085–1098.
[16] N. Leventis, Three-dimensional core-shell superstructures: Mechanically strong aerogels, Acc. Chem. Res. 40 (2007) 874–884.
[17] M.A.B. Meador, S.L. Vivod, L. McCorkle, D. Quade, R.M. Sullivan, L.J. Ghosn, N. Clark, L.A. Capadona, Reinforcing polymer cross-linked aerogels with carbon nanofibers, J. Mater. Chem. 18 (2008) 1843–1852.
[18] Z. Li, X. Cheng, S. He, X. Shi, L. Gong, H. Zhang, Aramid fibers reinforced silica aerogel composites with low thermal conductivity and improved mechanical performance, Compos. PT. A-Appl. Sci. Manuf. 84 (2016) 316–325.
[19] J. Cai, S. Liu, J. Feng, S. Kimura, M. Wada, S. Kuga, L. Zhang, Cellulose-silica nanocomposite aerogels by in situ formation of silica in cellulose gel, Angew. Chem. Int. Ed. 51 (2012) 2076–2079.
[20] H. Sai, L. Xing, J. Xiang, L. Cui, J. Jiao, C. Zhao, Z. Li, F. Li, T. Zhang, Flexible aerogels with interpenetrating network structure of bacterial cellulose-silica composite from sodium silicate precursor via freeze drying process, RSC Adv. 4 (2014) 30453–30461.
[21] N. Gupta, W. Ricci, Processing and compressive properties of aerogel/epoxy composites, J. Mater. Process. Technol. 198 (2008) 178–182.
[22] H.M. Kim, Y.J. Noh, J. Yu, S.Y. Kim, J.R. Youn, Silica aerogel/polyvinyl alcohol (PVA) insulation composites with preserved aerogel pores using interfaces between the superhydrophobic aerogel and hydrophilic PVA solution, Compos. PT. A-Appl. Sci. Manuf. 75 (2015) 39–45.
[23] J.W. Ju, T.M. Chen, Micromechanics and effective moduli of elastic composites containing randomly dispersed ellipsoidal inhomogeneities, Acta Mech. 103 (1994) 103–121.

[24] C. Buratti, E. Moretti, Glazing systems with silica aerogel for energy savings in buildings, Appl. Energy 98 (2012) 396–403.
[25] G. Wei, Y. Liu, X. Zhang, F. Yu, X. Du, Thermal conductivities study on silica aerogel and its composite insulation materials, Int. J. Heat Mass Tran. 54 (2011) 2355–2366.
[26] H. Hatta, M. Taya, Effective thermal conductivity of a misoriented short fiber composite, J. Appl. Phys. 58 (1985) 2478–2486.
[27] H. Hatta, M. Taya, Equivalent inclusion method for steady state heat conduction in composites, Int. J. Eng. Sci. 24 (1986) 1159–1172.
[28] S.Y. Kim, H.G. Jang, C.M. Yang, B.J. Yang, Multiscale prediction of thermal conductivity for nanocomposites containing crumpled carbon nanofillers with interfacial characteristics, Compos. Sci. Technol. 155 (2018) 169–176.
[29] L.-Y. Yu, Z.-L. Xu, H.-M. Shen, H.J. Yang, Prepared and characterization of PVDF-SiO2 composite hollow fiber UF membrane by sol-gel method, J. Membrane Sci. 337 (2009) 257–265.
[30] Z.-Q.X.-H. Dong, Z.-L. Ma, Z.-Y. Xu, Gu Superhydrophobic modification of PVDF-SiO2 electrospun nanofiber membranes for vacuum membrane distillation, RSC Adv. 5 (2015) 67962–67970.
[31] Z. Han, A. Fina, Thermal conductivity of carbon nanotubes and their polymer nanocomposites: a review, Prog. Polym. Sci. 36 (2011) 914–944.
[32] S.Y. Pak, H.M. Kim, S.Y. Kim, J.R. Youn, Synergistic improvement of thermal conductivity of thermoplastic composites with mixed boron nitride and multi-walled carbon nanotube fillers, Carbon 50 (2012) 4830–4838.
[33] H.S. Kim, H.S. Bae, J. Yu, S.Y. Kim, Thermal conductivity of polymer composites with the geometrical characteristics of graphene nanoplatelets, Sci. Rep. 6 (2016) 26825.
[34] Y. Xu, D.D.L. Chung, C. Mroz, Thermally conducting aluminum nitride polymer-matrix composites, Compos. Part A-Appl. S. 32 (2001) 1749–1757.
[35] C.J. Buchko, L.C. Chen, Y. Shen, D.C. Martin, Processing and microstructural characterization of porous biocompatible protein polymer thin films, Polymer 40 (1999) 7397–7407.